Analysis of stability and Hopf bifurcation of delayed feedback spin stabilization of a rigid spacecraft

Morad Nazari · Eric A. Butcher

Abstract The stability and bifurcation of delayed feedback spin stabilization of a rigid spacecraft is investigated in this paper. The spin is stabilized about the principal axis of the intermediate moment of inertia using a simple delayed feedback control law. In particular, linear stability is analyzed via the exponential-polynomial characteristic equations and then the method of multiple scales is used to obtain the normal form of the Hopf bifurcation. Bifurcation diagrams and the dynamics of the delayed closed-loop system are verified using continuation software and with numerical simulations.

1 Introduction

The subject of spin stabilization of spacecraft is of great significance in spacecraft design and attitude control. While the spin motion of rigid spacecraft is stable about the principal axes of minor and major inertia in the absence of external moments and internal

M. Nazari (✉) · E.A. Butcher
Department of Mechanical and Aerospace Engineering, New Mexico State University, Las Cruces, NM 88003, USA
e-mail: mozari82@yahoo.com

energy dissipation, the natural instability of the principal axis of intermediate inertia justifies the necessity for using a controller in order to stabilize intermediate axis spin. On the other hand, due to time delay in the sensors (e.g. rate gyros) or actuators (e.g. reaction control thrusters, control moment gyros, or reaction wheels), the current states are unlikely to be available for state feedback. Therefore, a delayed feedback control law is investigated in this work to simulate the more realistic situation of delayed spin stabilization.

There have been a few studies on the application of time delay in the feedback control of a rigid body for stability enhancement purposes. In [1, 2] discrete and distributed time delay were included, respectively, into Euler's equations of motion, where the equations of motion were obtained based on the Hamiltonian function. The method of multiple scales was employed in [3–5] to study the attitude dynamics of a spacecraft in the orbital plane, where a closed-loop control law was designed for the spacecraft using a magnetic control torque compared to which the gravity gradient torque is negligible in magnitude. In [6], equations of rotational motion were solved using the multiple scales approach and a limit process matching technique was implemented to allow the differential equations to be numerically integrated. The asymptotic solution was used to determine the time required to bring the spacecraft to a situation where there is only slight wobbling which can be removed by adding a nutation damper. Recently, the Lyapunov–Krasovskii functional [7, 8] and the inverse dynamics approach [9]

were used for the stability analysis of spacecraft with time delay in the measurement (i.e. [7, 8]) or in the actuators (i.e. [9]).

The normal form of a nonlinear system is the simplest possible form which yields the same qualitative dynamics as does the original system [10]. Many techniques such as the averaging method [11] and the Lyapunov–Floquet transformation (for time periodic equations) [12] have been used to obtain the normal forms for dynamical systems. However, two techniques, namely center manifold reduction and multiple scales method, are commonly used to obtain the normal forms of systems of delayed differential equations (DDEs). Center manifold reduction [13–15] and the multiple scales method [13, 16] are implemented for DDEs in the vicinity of Hopf bifurcations, in particular, by eliminating the fast dynamics. A noticeable advantage of the multiple scales method compared to center manifold reduction is that the former can be applied directly to infinite dimensional DDEs, whereas DDEs need to be converted into operator differential equations in a Banach space in order for the center manifold reduction technique to be applicable. It is demonstrated in [13] that the two techniques result in the same normal form of the bifurcation, although the computations involved in the method of multiple scales are significantly simpler.

In this study, the spin stabilization of a rigid spacecraft about an equilibrium state, which can be about any of the principal axes of the spacecraft, is considered. However, we specifically concentrate on the spin about the centroidal principal axis of intermediate moment of inertia, i.e. the intermediate spin which is generally unstable if no controller is used. The system is supplied with a linear delayed feedback control for stabilization purposes. The stability and bifurcation of the system is studied and compared with results from continuation software and numerical simulations. For this purpose, the method of multiple time scales is employed to provide the normal form of the Hopf bifurcation. It is found that when a non-delayed feedback controller is employed, a sufficiently large control gain globally asymptotically stabilizes the system, whereas when a delayed feedback controller is employed the control gain must be within a finite range in order for the system to be stable. Finally, simulations are provided to characterize the stable branches obtained by the continuation software and a period-doubling route to chaos is observed for time delays slightly more than 1 s.

2 Problem definition

The controlled angular velocity of a rigid spacecraft is obtained by adding a linear delayed feedback control to Euler's equations of a rigid body, i.e.

$$\mathbf{J}\dot{\boldsymbol{\omega}}(t) = -\boldsymbol{\omega}^{\times}(t)\mathbf{J}\boldsymbol{\omega}(t) + \mathbf{u}(t), \tag{1}$$

where $\mathbf{J}$ is the 3×3 body inertia matrix in principal coordinates, $\boldsymbol{\omega}(t) \in \mathbb{R}^3$ is the angular velocity in the body frame, and $\mathbf{u}(t) \in \mathbb{R}^3$ is the control torque. We aim to stabilize a desired nominal constant angular velocity $\boldsymbol{\Omega} \in \mathbb{R}^3$ about one of the principal axes using a delayed feedback control of the form

$$\mathbf{u}(t) = -\kappa \mathbf{x}(t - \tau), \tag{2}$$

where $\mathbf{x}(t) \in \mathbb{R}^3$ is the error in angular velocity of the system when compared to the nominal angular velocity ($\mathbf{x} = \boldsymbol{\omega} - \boldsymbol{\Omega}$), τ represents the time delay, and κ is the scalar control gain. Note that $(.)^{\times}: \mathbb{R}^3 \rightarrow \mathrm{so}(3)$ is the skew-symmetric mapping given by

$$\boldsymbol{\Psi}^{\times} = \begin{bmatrix} 0 & -\Psi_3 & \Psi_2 \\ \Psi_3 & 0 & -\Psi_1 \\ -\Psi_2 & \Psi_1 & 0 \end{bmatrix}, \tag{3}$$

where the space of 3×3 real skew-symmetric matrices is denoted by so(3), the Lie algebra of the Lie group SO(3). Substituting Eq. (2) into Eq. (1) the closed-loop dynamics of the rigid body with the delayed feedback control is obtained as

$$\dot{\mathbf{x}}(t) = \mathbf{L}\mathbf{x}(t) - \kappa \mathbf{M}\mathbf{x}(t - \tau) + \mathbf{R}(\mathbf{x}(t))$$
$$\triangleq \mathbf{F}(\mathbf{x}(t), \mathbf{x}(t - \tau), \kappa), \tag{4}$$

where

$$\mathbf{L} = \mathbf{J}^{-1}[-\boldsymbol{\Omega}^{\times}\mathbf{J} + (\mathbf{J}\boldsymbol{\Omega})^{\times}],$$
$$\mathbf{M} = \mathbf{J}^{-1}, \qquad \mathbf{R}(\mathbf{x}(t)) = -\mathbf{J}^{-1}\mathbf{x}^{\times}(t)\mathbf{J}\mathbf{x}(t).$$

3 Linear stability analysis

3.1 Characteristic equation

We assume the nominal motion of the spacecraft is to be uniformly spinning about one of its principal axes. There are six equilibrium points, two for each principal axis, in the spin dynamics of a rigid body. If the

nominal rotation is considered about the first principal axis, i.e.

$$\boldsymbol{\Omega} = \Omega_1 \boldsymbol{b}_1, \tag{5}$$

where $\boldsymbol{b}_1$ is the direction of the first principal axis in the body frame, then the matrix $\mathbf{L}$ takes the following form:

$$\mathbf{L} = \begin{bmatrix} 0 & 0 & 0 \\ 0 & 0 & \frac{J_3 - J_1}{J_2}\Omega_1 \\ 0 & \frac{J_1 - J_2}{J_3}\Omega_1 & 0 \end{bmatrix}. \tag{6}$$

To determine the type of bifurcation of the trivial solution $(\mathbf{0}, \kappa)$, we linearize Eq. (4), and study the roots of the characteristic equation $|\lambda \mathbf{I}_3 - \mathbf{L} + \kappa e^{-\lambda \tau}\mathbf{M}| = 0$, where $\mathbf{I}_3$ is the 3×3 identity matrix, $\lambda = \sigma + j\gamma$, σ corresponds to the non-oscillatory part of the solution, and γ is the frequency of oscillations. This results in the first order (decoupled) and the second order (coupled) equations

$$\lambda + \frac{1}{J_1}\kappa e^{-\lambda \tau} = 0, \tag{7a}$$

$$\lambda^2 + k_d e^{-\lambda \tau}\lambda + k_p e^{-2\lambda \tau} + \alpha_0 = 0, \tag{7b}$$

where

$$k_p = \frac{\kappa^2}{J_2 J_3}, \qquad k_d = \kappa\left(\frac{1}{J_2} + \frac{1}{J_3}\right),$$
$$\alpha_0 = \frac{(J_1 - J_3)(J_1 - J_2)}{J_2 J_3}\Omega_1^2. \tag{8}$$

Setting $\lambda = \sigma + j\gamma$, we can write

$$\sigma^2 + 2j\sigma\gamma - \gamma^2$$
$$+ k_d(\sigma + j\gamma)\left(e^{-\sigma\tau}\right)(\cos\gamma\tau - j\sin\gamma\tau)$$
$$+ k_p\left(e^{-2\sigma\tau}\right)(\cos 2\gamma\tau - j\sin 2\gamma\tau) + \alpha_0 = 0. \tag{9}$$

The system becomes unstable when the eigenvalues leave the left half complex plane at the critical value $\kappa = \kappa_c$. The critical frequency γ_c corresponds to the critical control gain κ_c at the stability boundary. We set $\sigma = 0$ in Eq. (9) to locate the stability boundary. Then, the complex-valued characteristic equation upon separating the real and imaginary parts can be obtained as

$$\text{Re}: \quad -\gamma^2 + k_d\gamma\sin\gamma\tau + k_p\cos 2\gamma\tau + \alpha_0 = 0, \tag{10a}$$

$$\text{Im}: \quad \gamma = \frac{2\kappa}{J_2 + J_3}\sin\gamma\tau. \tag{10b}$$

Hence, γ_c can be implicitly obtained via (see the Appendix)

$$\gamma_c^2\left[1 - \frac{(J_2 + J_3)^2}{J_2 J_3}\frac{1}{4\sin^2\gamma_c\tau}\right] = \alpha_0, \tag{11}$$

or, it can be obtained in terms of κ_c as (see the Appendix)

$$\gamma_c^2 = \frac{1}{J_2 J_3}\left[\kappa_c^2 + \Omega_1^2(J_3 - J_1)(J_2 - J_1)\right]$$
$$= k_{pc} + \alpha_0, \tag{12}$$

where k_{pc} denotes the critical value of k_p at the stability boundary.

To determine the type of bifurcation, $\frac{d\lambda}{d\kappa}$ is evaluated at $(\lambda, \kappa) = (i\gamma_c, \kappa_c)$, where the subscript c denotes the critical value, as

$$\frac{d\lambda}{d\kappa} = -\left\{\left(\frac{1}{J_2} + \frac{1}{J_3}\right)\lambda e^{-\lambda\tau} + \frac{2\kappa}{J_2 J_3}e^{-2\lambda\tau}\right\}$$
$$\times \left\{2\lambda + \kappa\left(\frac{1}{J_2} + \frac{1}{J_3}\right)e^{-\lambda\tau}\right.$$
$$- \tau\lambda\kappa\left(\frac{1}{J_2} + \frac{1}{J_3}\right)e^{-\lambda\tau}$$
$$\left. - 2\tau\frac{\kappa^2}{J_2 J_3}e^{-2\lambda\tau}\right\}^{-1} \tag{13}$$

whose real part at the critical point is nonzero, i.e.

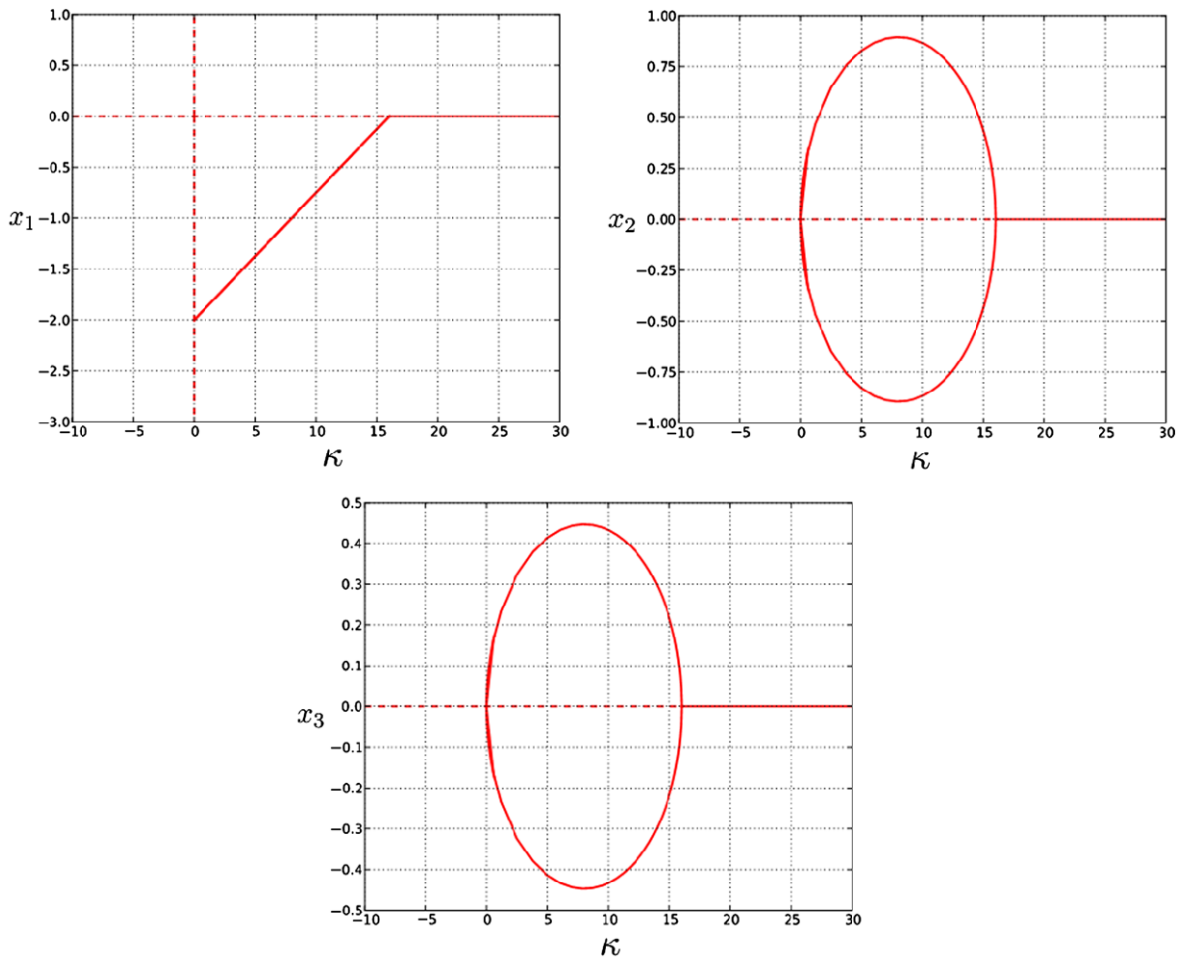$$\lim_{\kappa \to \kappa_c}\text{Re}\left(\frac{d\lambda}{d\kappa}\right) = \lim_{\kappa \to \kappa_c}\frac{\text{Num}}{\text{Den}} \neq 0, \tag{14}$$

where

Num

$$= 2\kappa_c^2\left[-(J_2 + J_3)\cos\gamma_c\tau + 2\tau\kappa_c\right]$$
$$- (J_2 + J_3)\gamma_c^2\left[2J_2 J_3\cos\gamma_c\tau - (J_2 + J_3)\kappa_c\tau\right]$$
$$- 4\gamma_c\kappa_c\left[-2J_2 J_3\cos\gamma_c\tau + (J_2 + J_3)\tau\kappa_c\right]\sin\gamma_c\tau$$
$$= 2\kappa_c^2\left[-(J_2 + J_3)\cos\gamma_c\tau + 2\kappa_c\tau\right]$$
$$= \frac{2\gamma\tau - \sin 2\gamma\tau}{\sin\gamma\tau}\kappa^2(J_2 + J_3) \neq 0,$$

Den

$$= \kappa_c^2\left[(J_2 + J_3)^2 - 4(J_2 + J_3)\tau\kappa_c\cos\gamma_c\tau + 4\tau^2\kappa_c^2\right]$$

Fig. 1 Bifurcation diagrams of the non-delayed feedback control for the inertia matrix $\mathbf{J} = \text{diag}[14, 10, 30]$ kg.m^2 and nominal spin rate $\Omega_1 = 2 \frac{\text{rad}}{\text{s}}$. The stable and unstable branches are shown with *solid* and *dashed lines*, respectively

$$+ \kappa_c^2 \left[1 + \left(\frac{\Omega_1}{\kappa_c} \right)^2 (J_3 - J_1)(J_2 - J_1) \right]$$

$$\times \left[-2(J_2^2 + J_3^2) + 4(J_2 + J_3)\tau\kappa_c \cos\gamma_c\tau \right.$$

$$\left. - \frac{(J_2 + J_3)^2}{J_2 J_3} \tau^2 \kappa_c^2 \right]$$

$$= -\kappa_c^2 (J_2 - J_3)^2 \left(1 + \frac{\tau^2 \kappa_c^2}{J_2 J_3} \right)$$

$$+ \Omega_1^2 (J_1 - J_3)(J_1 - J_2) \left[-2(J_2^2 + J_3^2) \right.$$

$$\left. + 4(J_2 + J_3)\tau\kappa_c \cos\gamma_c\tau - \frac{(J_2 + J_3)^2}{J_2 J_3} \tau^2 \kappa_c^2 \right]. \tag{15}$$

Since the eigenvalues $\lambda(\kappa)$ (λ as a function of κ) are continuously differentiable with respect to κ near to κ_c, and since $\text{Re}(\frac{d\lambda}{d\kappa}) \neq 0$, based on the Hopf bifurcation theory [17] the system exhibits the Hopf bifurcation. That is, the exchange of stability of the trivial solution is hyperbolic (non-degenerate).

3.2 Non-delayed case

To study the stability of the non-delayed system, the current state feedback is used, i.e. in Eq. (2) we set $\mathbf{u} = -\kappa\mathbf{x}(t)$. The characteristic equation given in Eq. (7b) simplifies to

$$\lambda^2 + k_d\lambda + k_p + \alpha_0 = 0 \tag{16}$$
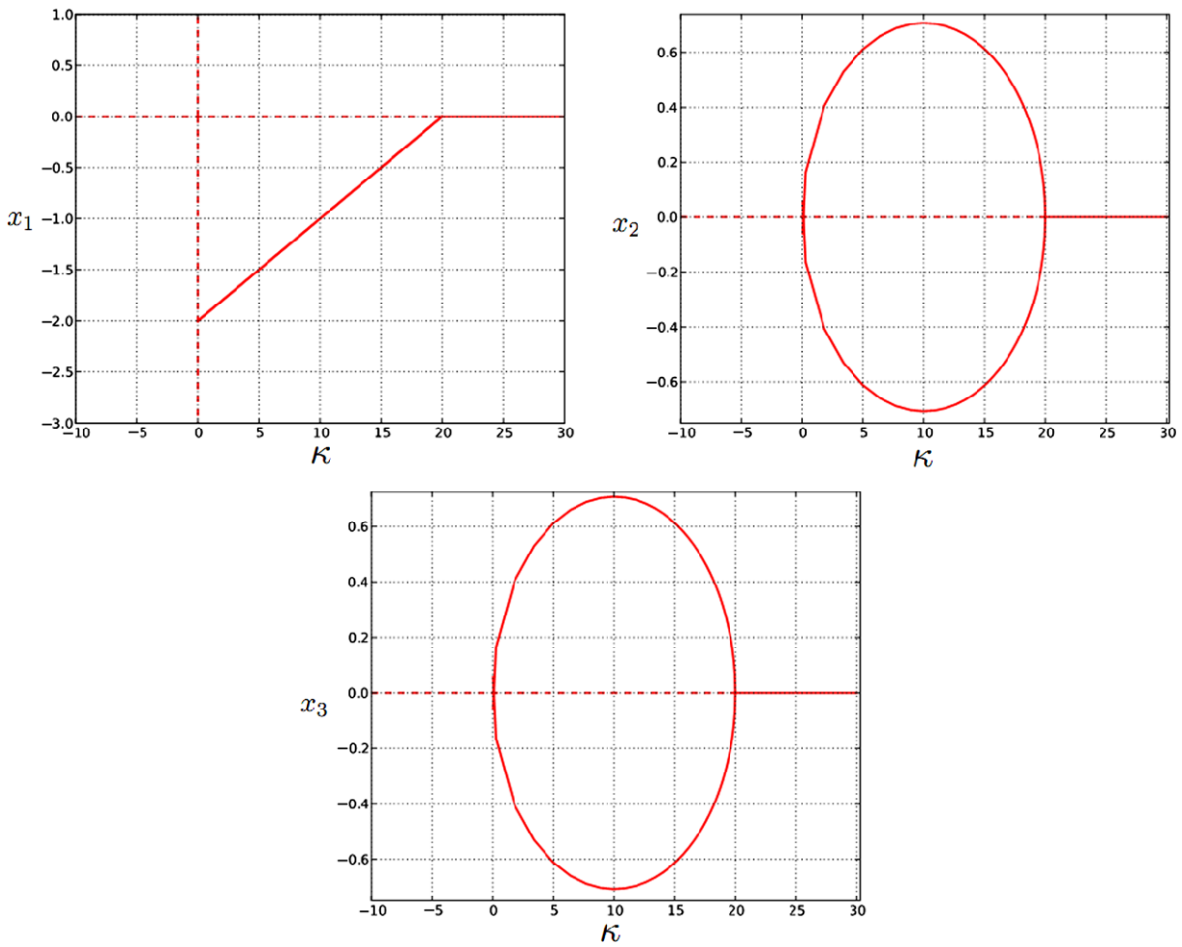
Fig. 2 Bifurcation diagrams of the non-delayed feedback control for the inertia matrix $\mathbf{J} = \mathrm{diag}[20, 10, 30]$ kg.m^2 and nominal spin rate $\Omega_1 = 2\,\frac{\mathrm{rad}}{\mathrm{s}}$. The stable and unstable branches are shown with *solid* and *dashed lines*, respectively

whose solution can be expressed as $\lambda = -C \pm \sqrt{B - A}$ where

$$A = \alpha_0, \qquad B = \frac{\kappa^2(J_2 - J_3)^2}{4(J_2 J_3)^2} = \left(\frac{k_d}{2}\right)^2 - k_p,$$

$$C = \frac{\kappa}{2}\left(\frac{J_2 + J_3}{J_2 J_3}\right) = \frac{k_d}{2}. \tag{17}$$

Knowing that $\sqrt{B} < C$ and that for both the minor spin ($J_1 < J_2, J_3$) and the major spin ($J_1 > J_2, J_3$) A is positive, we consider two cases: $0 < A < B$ or $A > B$. Under the first condition we have $\sqrt{B - A} < \sqrt{B} < C$, i.e. both roots of the characteristic equation (16) are real and negative. Under the second condition Eq. (16) has two complex roots with negative real parts. Thus, the major and minor spins are always stable for any values of κ (specifically $\kappa = 0$ for the

uncontrolled system), while the stability of the intermediate axis depends on the values of κ. Therefore, for the linearized spin motion about either the major axis ($J_1 > J_2, J_3$) or the minor axis ($J_1 < J_2, J_3$), a frequency $\gamma \in \mathbb{R}$ can always be found for any control gain value, whereas for the motion about the intermediate axis ($J_3 < J_1 < J_2$), the existence of $\gamma \in \mathbb{R}$ depends on the value of the control gain κ.

AUTO [18] is applied as the numerical continuation software to Eq. (4) with $\tau = 0$ to produce branches of equilibria for varying κ. The equilibrium points are displayed in the bifurcation diagrams given in Figs. 1–3 which imply that the system encounters supercritical pitchfork bifurcation. In Sect. 5, simulations are used to determine the type of bifurcation. It can be seen that there are no turning points between the bifurca-
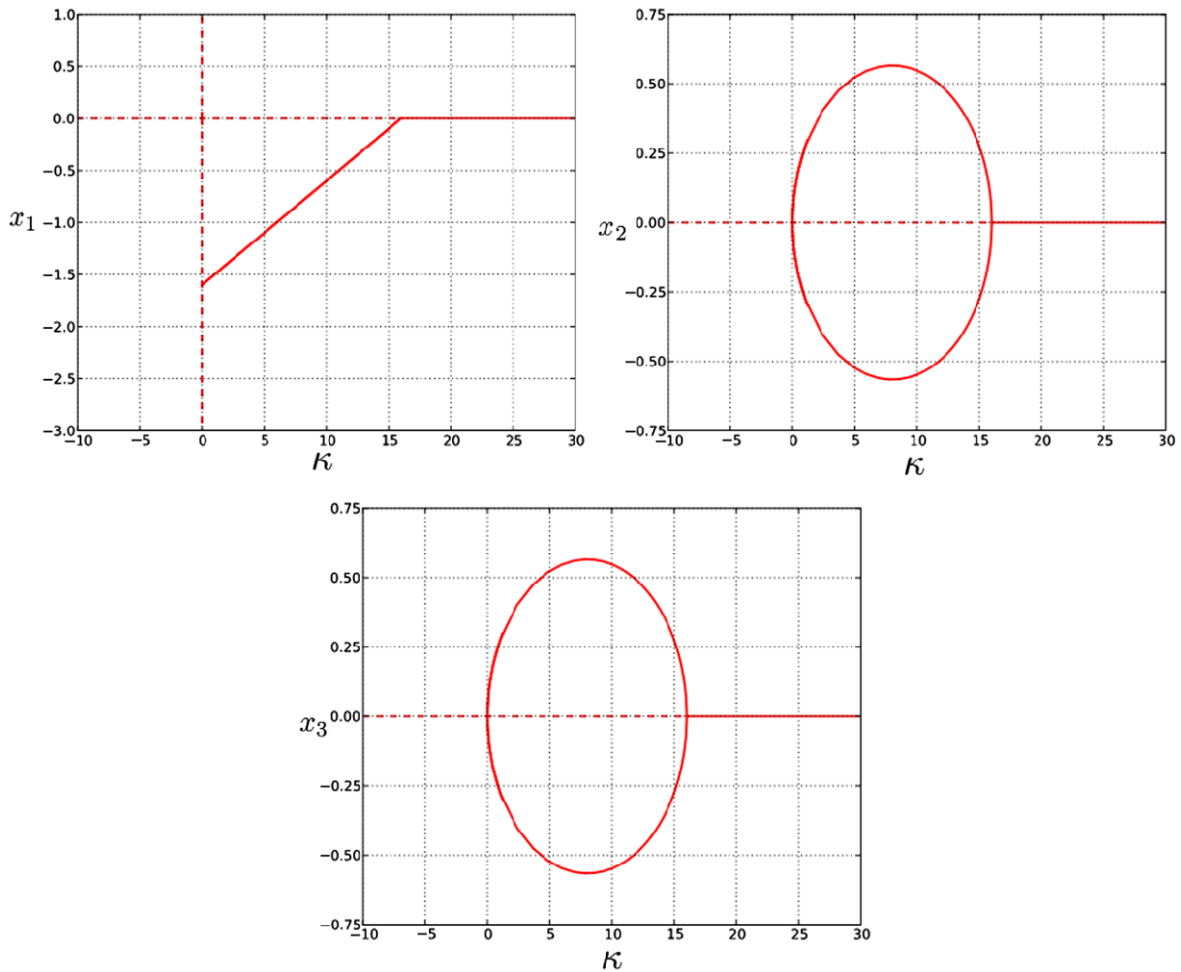
Fig. 3 Bifurcation diagrams of the non-delayed feedback control for the inertia matrix $\mathbf{J} = \text{diag}[20, 10, 30]$ kg.m^2 and nominal spin rate $\Omega_1 = 1.6 \frac{\text{rad}}{\text{s}}$. The stable and unstable branches are shown with *solid* and *dashed lines*, respectively

tion points and that nontrivial equilibrium points are entirely stable.

3.3 Delayed case

The stability condition of Eq. (7a) which corresponds to

$$\dot{x}(t) = ax(t - \tau), \tag{18}$$

where $a = -\frac{\kappa\tau}{J_1}$, can be obtained as

$$0 < \kappa < \frac{\pi J_1}{2\tau}. \tag{19}$$

Divergence and flutter instability boundaries are studied based on Eqs. (10a) and (10b). In order to obtain

the divergence boundary, we set $\gamma = 0$ which yields

$$k_p = -\alpha_0. \tag{20}$$

In order to obtain the flutter boundary, we set $\gamma \neq 0$ in Eqs. (10a) and (10b). Thus, in matrix form,
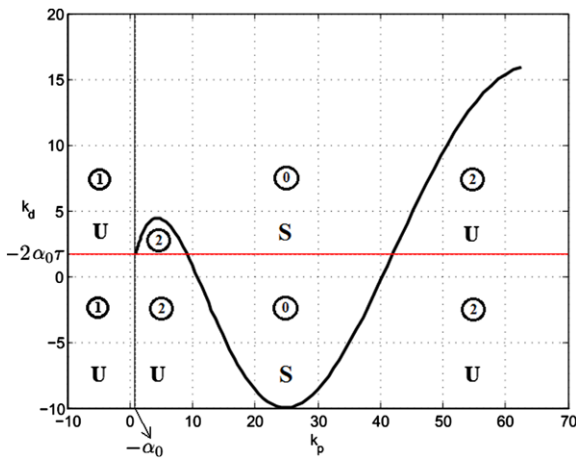
$$\begin{bmatrix} \cos 2\gamma\tau & \gamma \sin \gamma\tau \\ -\sin 2\gamma\tau & \gamma \cos \gamma\tau \end{bmatrix} \begin{bmatrix} k_p \\ k_d \end{bmatrix} = \begin{bmatrix} \gamma^2 - \alpha_0 \\ 0 \end{bmatrix}. \tag{21}$$

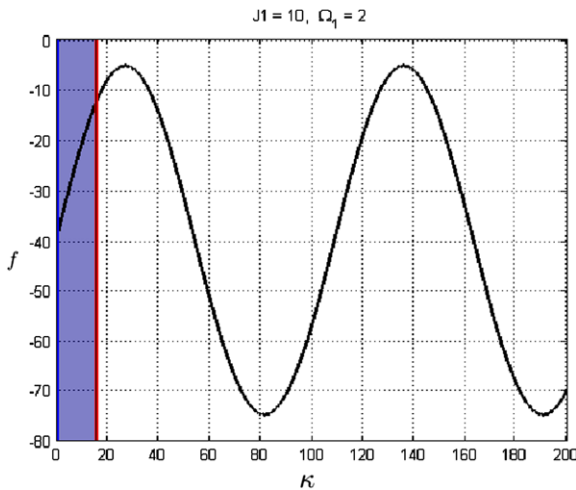From Eq. (21), the coefficients k_d and k_p can be obtained as

$$k_p = \gamma^2 - \alpha_0, \tag{22a}$$

$$k_d = \frac{2 \sin \gamma\tau}{\gamma}(\gamma^2 - \alpha_0). \tag{22b}$$

Fig. 4 Stability chart in the $k_p - k_d$ parameter plane indicating the number of unstable characteristic exponents with $\alpha_0 = -0.8533$ and $\tau = 1$ s. This figure corresponds to the second order coupled characteristic equation (7b). The stable and unstable regions are labeled by S and U, respectively
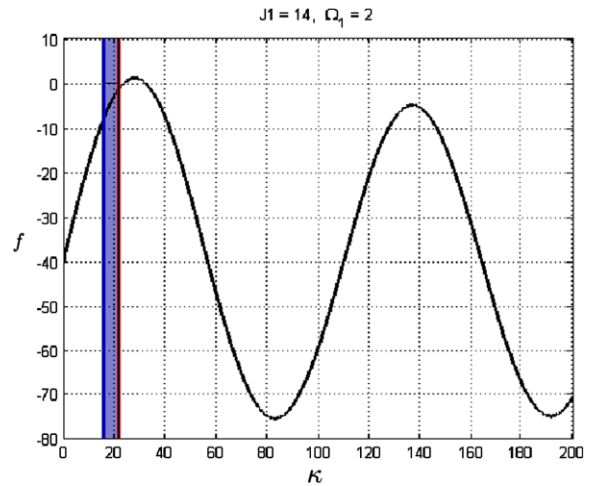

Fig. 6 Stability regions are shadowed for the inertia matrix $\mathbf{J} = \mathrm{diag}[14, 10, 30]$ kg.m^2, nominal spin rate $\Omega_1 = 2 \frac{\mathrm{rad}}{\mathrm{s}}$, and $\tau = 1$ s

Fig. 5 Stability regions are shadowed for the inertia matrix $\mathbf{J} = \mathrm{diag}[10, 10, 30]$ kg.m^2, nominal spin rate $\Omega_1 = 2 \frac{\mathrm{rad}}{\mathrm{s}}$, and $\tau = 1$ s

Fig. 7 Stability regions are shadowed for the inertia matrix $\mathbf{J} = \mathrm{diag}[19, 10, 30]$ kg.m^2, nominal spin rate $\Omega_1 = 2 \frac{\mathrm{rad}}{\mathrm{s}}$, and $\tau = 1$ s
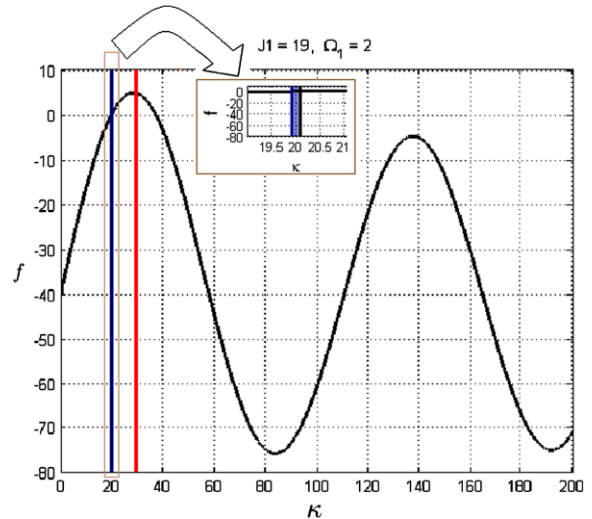
Following [19], taking the partial derivative of Eq. (9) with respect to k_p and recalling Eqs. (22a) and (22b) when $\gamma = 0$, we can obtain

$$\frac{\partial \sigma}{\partial k_p} = -\frac{1}{k_d + 2\alpha_0 \tau}. \tag{23}$$

If $k_d > -2\alpha_0\tau$ then $\frac{\partial \sigma}{\partial k_p} < 0$, and if $k_d < -2\alpha_0\tau$ then $\frac{\partial \sigma}{\partial k_p} > 0$. Therefore, if the line $k_p = -\alpha_0$ is crossed from left to right and $k_d > -2\alpha_0\tau$, then a real
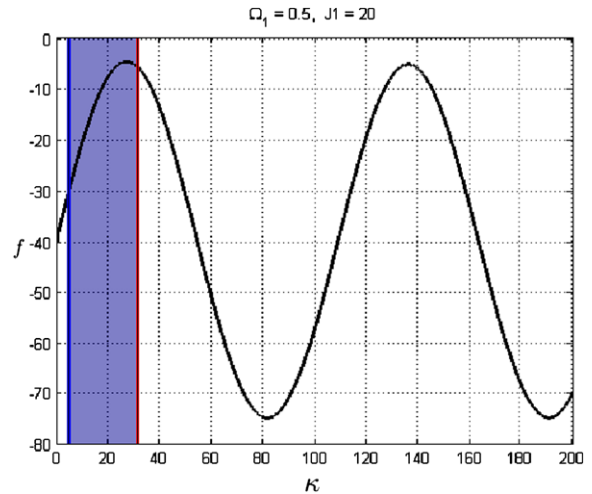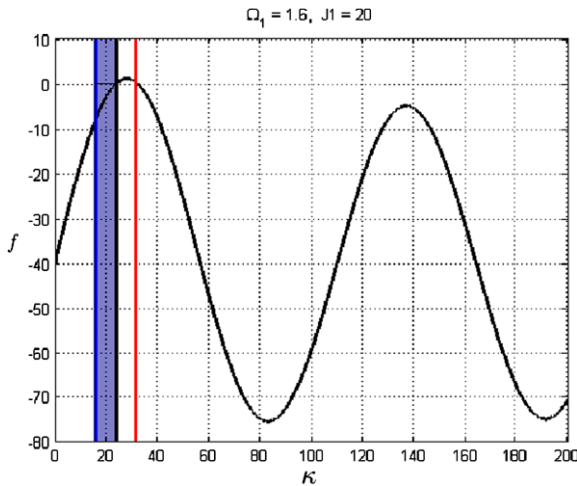
characteristic exponent becomes stable. Whereas, if the line $k_p = -\alpha_0$ is crossed from left to right and $k_d < -2\alpha_0\tau$, then a real characteristic exponent becomes unstable. On the other hand, from Eq. (7b), it is clear that for $\alpha_0 < 0$, there is an unstable real eigenvalue if $k_d = k_p = 0$. Hence, the origin in the $k_p - k_d$ parameter plane has one real positive characteristic exponent. Based on this fact, and by considering the exponent-crossing directions along $k_p = -\alpha_0$ the number of unstable eigenvalues can be obtained. The
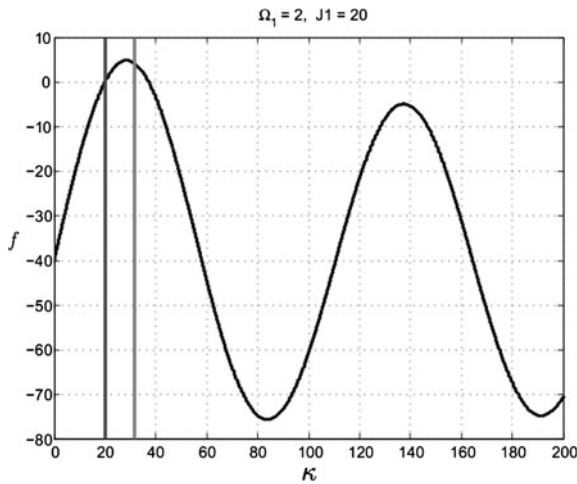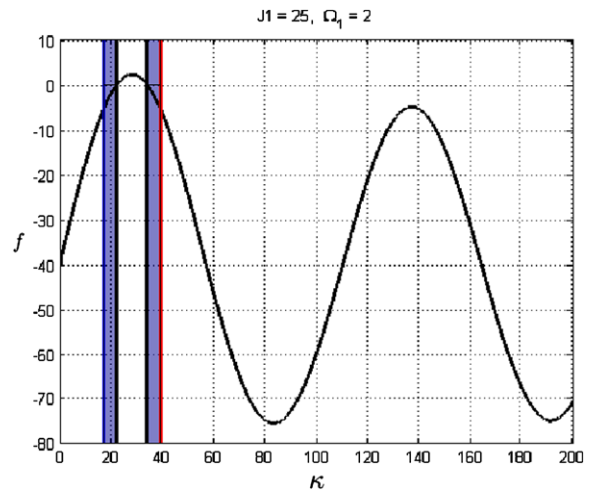
Fig. 8 Stability regions are shadowed for the inertia matrix $\mathbf{J} = \mathrm{diag}[20, 10, 30]$ kg.m^2, nominal spin rate $\Omega_1 = 2$ $\frac{\mathrm{rad}}{\mathrm{s}}$, and $\tau = 1$ s

Fig. 9 Stability regions are shadowed for the inertia matrix $\mathbf{J} = \mathrm{diag}[20, 10, 30]$ kg.m^2, nominal spin rate $\Omega_1 = 1.6$ $\frac{\mathrm{rad}}{\mathrm{s}}$, and $\tau = 1$ s

Fig. 10 Stability regions are shadowed for the inertia matrix, $\mathbf{J} = \mathrm{diag}[20, 10, 30]$ kg.m^2, nominal spin rate $\Omega_1 = 0.5$ $\frac{\mathrm{rad}}{\mathrm{s}}$, and $\tau = 1$ s

Fig. 11 Stability regions are shadowed for the inertia matrix, $\mathbf{J} = \mathrm{diag}[25, 10, 30]$ kg.m^2, nominal spin rate $\Omega_1 = 2$ $\frac{\mathrm{rad}}{\mathrm{s}}$, and $\tau = 1$ s
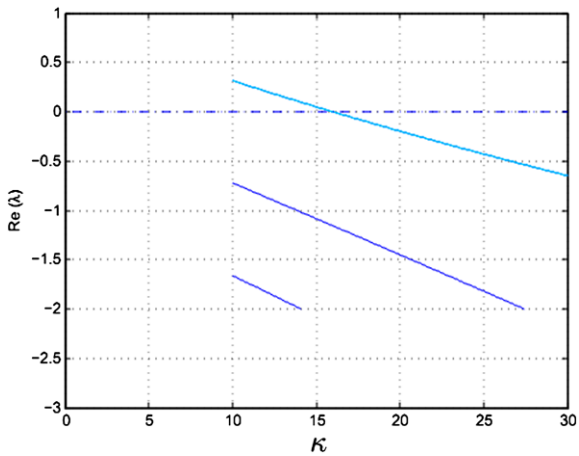
result for the inertia matrix $\mathbf{J} = \mathrm{diag}[14, 10, 30]$ kg.m^2 and the nominal spin rate $\Omega_1 = 2$ $\frac{\mathrm{rad}}{\mathrm{s}}$ is shown in Fig. 4, where the thick black curve is associated with the flutter instability boundary and the vertical line $k_p = -\alpha_0$ corresponds to the divergence instability boundary. The numbers of unstable characteristic exponents are mentioned inside circles for different regions in Fig. 4. Solving Eq. (22a) for γ and substituting it into Eq. (22b), the explicit relation between k_p and k_d can be obtained. According to Fig. 4, after writing k_d in terms of k_p using Eqs. (22a) and (22b),

it can be shown that the stable regions corresponding to Eq. (7b) in the $(k_p - k_d)$ parameter plane can be described by
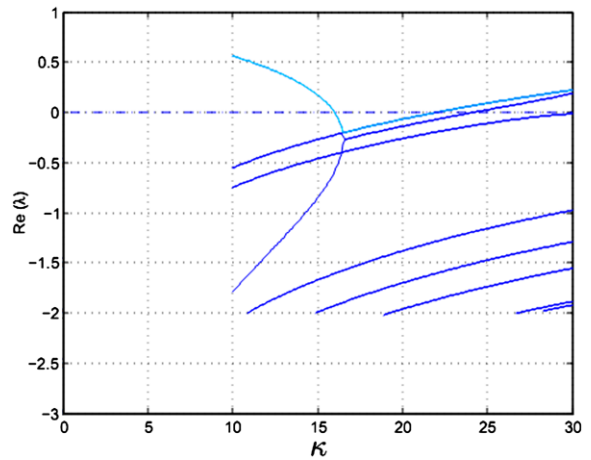
$$k_p > -\alpha_0, \qquad k_d > \frac{2\sin(\tau\sqrt{k_p + \alpha_0})}{\sqrt{k_p + \alpha_0}} k_p. \qquad (24)$$

Now, we use Eq. (8) to write k_p, k_d, and α_0 in terms of the system moments of inertia and the control gain κ. The delay independent stability condition of system with delayed feedback control given in Eq. (1) can be
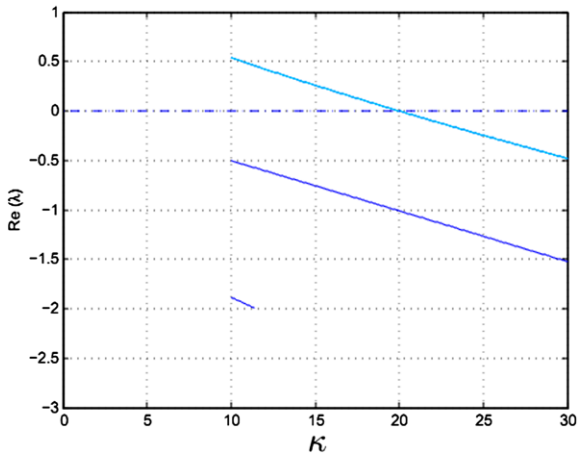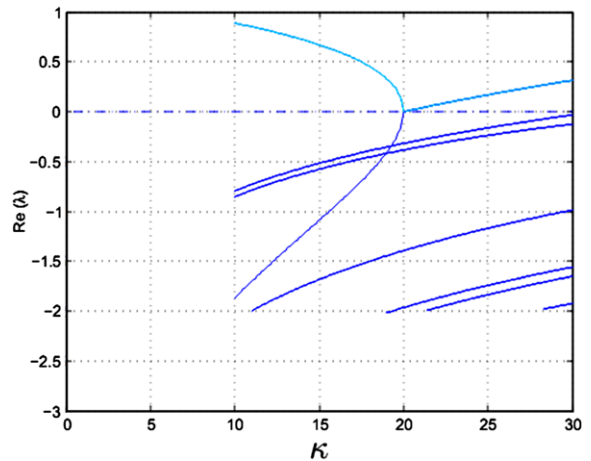
Fig. 12 Eigenvalues real part for different values of κ_c for the inertia matrix $\mathbf{J} = \mathrm{diag}[14, 10, 30]$ kg.m^2, nominal spin rate $\Omega_1 = 2 \frac{\mathrm{rad}}{\mathrm{s}}$, and $\tau = 0.01$ s

Fig. 14 Eigenvalues real part for different values of κ_c for the inertia matrix $\mathbf{J} = \mathrm{diag}[14, 10, 30]$ kg.m^2, nominal spin rate $\Omega_1 = 2 \frac{\mathrm{rad}}{\mathrm{s}}$, and $\tau = 1$ s

Fig. 13 Eigenvalues real part for different values of κ_c for the inertia matrix $\mathbf{J} = \mathrm{diag}[20, 10, 30]$ kg.m^2, nominal spin rate $\Omega_1 = 2 \frac{\mathrm{rad}}{\mathrm{s}}$, and $\tau = 0.01$ s

Fig. 15 Eigenvalues real part for different values of κ_c for the inertia matrix $\mathbf{J} = \mathrm{diag}[20, 10, 30]$ kg.m^2, nominal spin rate $\Omega_1 = 2 \frac{\mathrm{rad}}{\mathrm{s}}$, and $\tau = 1$ s

obtained from Eq. (24) as

$$\mathbf{S}_i = \{\kappa \mid \kappa > \sqrt{-\alpha_0 J_2 J_3} \text{ or } \kappa < -\sqrt{-\alpha_0 J_2 J_3}\}. \quad (25)$$

Also, according to Eqs. (19) and (24), the delay dependent stability condition can be obtained as

$$\mathbf{S}_d = \left\{\kappa \mid f(\kappa, \tau) < 0 \text{ and } 0 < \kappa < \frac{\pi J_1}{2\tau}\right\}, \quad (26)$$

where

$$f(\kappa, \tau) = 2\kappa \frac{\sin\left(\tau\sqrt{\frac{\kappa^2}{J_2 J_3} + \alpha_0}\right)}{\sqrt{\frac{\kappa^2}{J_2 J_3} + \alpha_0}} - (J_2 + J_3). \quad (27)$$

Note that, according to Eq. (8), $\frac{\kappa^2}{J_2 J_3}$ in Eq. (27) is the same as k_p.

4 Normal form of Hopf bifurcation

To obtain the normal form of the Hopf bifurcation, we define the detuning parameter δ as

$$\kappa = \kappa_c + \epsilon^2 \delta, \tag{28}$$

which quantifies the closeness of the feedback control gain κ to its critical value κ_c. Then, we let

$$\mathbf{x}(t; \epsilon) = \epsilon \mathbf{x}_1(T_0, T_2) + \epsilon^2 \mathbf{x}_2(T_0, T_2)$$
$$+ \epsilon^3 \mathbf{x}_3(T_0, T_2) + \cdots, \tag{29}$$

where $T_0 = t$, $T_2 = \epsilon^2 t$, and ϵ is the bookkeeping parameter. The solution does not depend on T_1 since secular terms that cause resonance first appear at $O(\epsilon^3)$. The time derivative with respect to t can then be expressed as

$$\frac{d}{dt} = \frac{\partial}{\partial T_0} + \epsilon^2 \frac{\partial}{\partial T_2} + \cdots = D_0 + \epsilon^2 D_2 + \cdots. \tag{30}$$

The Taylor series expansion is utilized for small ϵ to express the delayed term $\mathbf{x}(t - \tau)$ as

$$\mathbf{x}(t - \tau; \epsilon)$$
$$= \epsilon \mathbf{x}_1(T_0 - \tau, T_2 - \epsilon^2 \tau) + \epsilon^2 \mathbf{x}_2(T_0 - \tau, T_2 - \epsilon^2 \tau)$$
$$+ \epsilon^3 \mathbf{x}_3(T_0 - \tau, T_2 - \epsilon^2 \tau) + \cdots$$
$$= \epsilon \mathbf{x}_{1\tau} + \epsilon^2 \mathbf{x}_{2\tau} + \epsilon^3(-\tau D_2 \mathbf{x}_{1\tau} + \mathbf{x}_{3\tau}) + \cdots,$$

where $\mathbf{x}_\tau$ denotes $\mathbf{x}(T_0 - \tau, T_2)$.

Substituting Eqs. (28)–(30) into Eq. (4), and equating coefficients of like powers of ϵ, three sets of equations can be obtained as

$$\mathcal{L}\mathbf{x}_1 = \mathbf{0}, \tag{31a}$$

$$\mathcal{L}\mathbf{x}_2 = -\mathbf{J}^{-1}\mathbf{x}_1^\times \mathbf{J}\mathbf{x}_1, \tag{31b}$$

$$\mathcal{L}\mathbf{x}_3 = -D_2 \mathbf{x}_1 + \kappa_c \tau \mathbf{M} D_2 \mathbf{x}_{1\tau} - \delta \mathbf{M} \mathbf{x}_{1\tau}$$
$$- \mathbf{J}^{-1}(\mathbf{x}_1^\times \mathbf{J}\mathbf{x}_2 + \mathbf{x}_2^\times \mathbf{J}\mathbf{x}_1), \tag{31c}$$

where $\mathbf{x}$ denotes $\mathbf{x}(T_0, T_2)$, and the operator $\mathcal{L}$ is defined such that $\mathcal{L}\mathbf{x}_i = D_0 \mathbf{x}_i - \mathbf{L}\mathbf{x}_i + \kappa_c \mathbf{M}\mathbf{x}_{i\tau}$. The general solution for (31a) can be expressed as

$$\mathbf{x}_1 = A(T_2)\boldsymbol{\phi} e^{i\gamma_c T_0} + cc, \tag{32}$$

where cc denotes the complex conjugate of the preceding terms, and $\boldsymbol{\phi}$ is the eigenvector corresponding

to the eigenvalue $i\gamma_c$ which is a constant vector of the form

$$\boldsymbol{\phi} = \begin{bmatrix} \alpha \\ 1 \\ \phi_3 \end{bmatrix}, \quad \phi_3 = \frac{j\gamma_c J_2 + \kappa_c e^{-j\gamma_c \tau}}{(J_3 - J_1)\Omega_1}, \tag{33}$$

where α can be any complex value, and γ_c can be obtained from Eq. (11). Substituting Eq. (32) into Eq. (31b) and seeking for the particular solution for $\mathbf{x}_2$ yields

$$\mathbf{x}_2 = \boldsymbol{\Gamma}_1 A^2 e^{2i\gamma_c T_0} + \boldsymbol{\Gamma}_2 A\bar{A} + cc, \tag{34}$$

where $(\bar{\cdot})$ denotes the complex conjugate, and

$$\boldsymbol{\Gamma}_1 = \left(-2i\gamma_c \mathbf{I}_3 + \mathbf{L} - \kappa_c \mathbf{M}e^{-2i\gamma_c \tau}\right)^{-1}\mathbf{J}^{-1}\boldsymbol{\phi}^\times \mathbf{J}\boldsymbol{\phi},$$
$$\boldsymbol{\Gamma}_2 = (\mathbf{L} - \kappa_c \mathbf{M})^{-1}\mathbf{J}^{-1}\boldsymbol{\phi}^\times \mathbf{J}\bar{\boldsymbol{\phi}}. \tag{35}$$

Substituting Eqs. (32) and (34) into Eq. (31c) yields

$$\mathcal{L}\mathbf{x}_3 = \left(-\mathbf{I}_3 + \kappa_c \tau \mathbf{M}e^{-i\gamma_c \tau}\right)\boldsymbol{\phi} D_2 A e^{i\gamma_c T_0}$$
$$- \delta \mathbf{M}\boldsymbol{\phi} e^{-i\gamma_c \tau} A e^{i\gamma_c T_0}$$
$$- \mathbf{J}^{-1}\big[\boldsymbol{\phi}^\times \mathbf{J}(\boldsymbol{\Gamma}_2 + \bar{\boldsymbol{\Gamma}}_2) + \bar{\boldsymbol{\phi}}^\times \mathbf{J}\boldsymbol{\Gamma}_1 + \boldsymbol{\Gamma}^\times_1 \mathbf{J}\bar{\boldsymbol{\phi}}$$
$$+ \left(\boldsymbol{\Gamma}^\times_2 + \bar{\boldsymbol{\Gamma}}^\times_2\right)\mathbf{J}\boldsymbol{\phi}\big] A^2 \bar{A} e^{i\gamma_c T_0} + cc$$
$$+ \text{NST}, \tag{36}$$

where NST represents the terms that do not produce secular terms.

For the set of Eqs. (31a), (31b) and (31c) to have a solution it is necessary and sufficient that the solvability conditions are satisfied. Following a similar procedure as in [13], to eliminate the secular terms in Eq. (34), a particular solution of $\mathbf{x}_3$ is sought of the form $\mathbf{x}_3 = \boldsymbol{\Theta}(T_1, T_2)e^{i\gamma_c T_0}$ which, after substituting in Eq. (34), yields

$$\left(-i\gamma_c \mathbf{I}_3 + \mathbf{L} - \kappa_c e^{-i\gamma_c \tau}\mathbf{M}\right)\boldsymbol{\Theta}$$
$$= \left(\mathbf{I}_3 - \kappa_c \tau \mathbf{M}e^{-i\gamma_c \tau}\right)\boldsymbol{\phi} D_2 A + \delta \mathbf{M}\boldsymbol{\phi} e^{-i\gamma_c \tau} A$$
$$+ \mathbf{J}^{-1}\big[\boldsymbol{\phi}^\times \mathbf{J}(\boldsymbol{\Gamma}_2 + \bar{\boldsymbol{\Gamma}}_2) + \bar{\boldsymbol{\phi}}^\times \mathbf{J}\boldsymbol{\Gamma}_1 + \boldsymbol{\Gamma}_1^\times \mathbf{J}\bar{\boldsymbol{\phi}}$$
$$+ \left(\boldsymbol{\Gamma}^\times_2 + \bar{\boldsymbol{\Gamma}}^\times_2\right)\mathbf{J}\boldsymbol{\phi}\big] A^2 \bar{A}. \tag{37}$$

The solvability condition of the algebraic equation given in (37) requires that the right hand side of Eq. (37) be orthogonal to every solution of the adjoint (conjugate transpose) homogeneous problem

$$\left(i\gamma_c \mathbf{I}_3 + \mathbf{L}^* - \kappa_c e^{i\gamma_c \tau}\mathbf{M}^*\right)\mathbf{h} = \mathbf{0}, \tag{38}$$

where $(.)^*$ denotes the conjugate transpose, and, since $\mathbf{L}$ and $\mathbf{M}$ are real matrices, $\mathbf{L}^* = \mathbf{L}$ and $\mathbf{M}^* = \mathbf{M}$. Note that the same is true for $\mathbf{J}$, i.e. $\mathbf{J}^* = \mathbf{J}$. We refer the reader to [10, 20, 21] for more details on solvability conditions. To achieve a unique solution for $\mathbf{h}$ in Eq. (38), $\mathbf{h}$ is normalized as $\mathbf{h}^*.\boldsymbol{\phi} = 1$, and the complex value α is set to $\alpha = \phi_3$ in Eq. (33) for more convenience. Then, the solution of $\mathbf{h}$ can be obtained as $\mathbf{h} = [-\bar{\alpha}, 1, \bar{\alpha}]^T$, where $\bar{\alpha}$ denotes the complex conjugate of α. According to the orthogonality described above, if we set the inner product of $\mathbf{h}$ and the right hand side of Eq. (37) to zero and solve for $D_2 A$, the resulting complex-valued form of the normal form of the bifurcation can be obtained as

$$D_2 A = \delta \Lambda_1 A + \Lambda_2 A^2 \bar{A}, \tag{39}$$

where

$$
\begin{aligned}
\Lambda_1 = &-\left\{\alpha\bar{\alpha}J_2(J_1 - J_3) + J_1 J_3\right\}\left\{J_1 J_2 J_3\right. \\
&\left. - e^{-i\gamma_c\tau}\tau\kappa_c\left[\alpha\bar{\alpha}J_2(J_1 - J_3) + J_1 J_3\right]\right\}^{-1}e^{-i\gamma_c\tau},
\end{aligned}
$$

$$
\begin{aligned}
\Lambda_2 = &-\left\{\bar{\alpha}J_2 J_3(J_3 - J_2)\left(\frac{\chi_{11}}{\Xi_{11}} + \frac{\chi_{12}}{\Xi_{12}}\right)\right. \\
&+ \bar{\alpha}J_3 J_1(J_1 - J_3) \\
&\times \left(\frac{\chi_{21}}{\kappa_c} + \frac{\chi_{22}}{\Xi_{22}} + \frac{\chi_{23}}{\Xi_{23}} + \frac{\chi_{24}}{\Xi_{24}}\right) \\
&+ \bar{\alpha}J_1 J_2(J_2 - J_1) \\
&\times \left(\frac{\chi_{31}}{\kappa_c} + \frac{\chi_{32}}{\Xi_{32}} + \frac{\chi_{33}}{\Xi_{33}} + \frac{\chi_{34}}{\Xi_{34}}\right)\right\} \\
&\times \left\{J_1 J_2 J_3 - e^{-i\gamma_c\tau}\tau\kappa_c\right. \\
&\times \left[\alpha\bar{\alpha}J_2(J_1 - J_3) + J_1 J_3\right]\right\}^{-1},
\end{aligned}
\tag{40}
$$

where

$$
\begin{aligned}
\chi_{11} = &-\alpha(3\bar{\alpha} + \alpha)(J_2 - J_1)(J_1 - J_3)\Omega_1 \\
&+ \left[(\alpha + \bar{\alpha})(J_2 - J_1) + 2\alpha^2\bar{\alpha}(J_1 - J_3)\right]\kappa_c,
\end{aligned}
$$

$$\Xi_{11} = -(J_2 - J_1)(J_1 - J_3)\Omega_1^2 + \kappa_c^2,$$

$$
\begin{aligned}
\chi_{12} = &\, e^{2i\gamma_c\tau}\alpha\left\{-e^{2i\gamma_c\tau}(J_2 - J_1)(J_1 - J_3)(\alpha + \bar{\alpha})\Omega_1\right. \\
&+ 2ie^{2i\gamma_c\tau}\left[J_2(J_2 - J_1) + \alpha\bar{\alpha}J_3(J_1 - J_3)\right]\gamma_c \\
&\left. + \left[(J_2 - J_1) + \alpha\bar{\alpha}(J_1 - J_3)\right]\kappa_c\right\},
\end{aligned}
$$

$$\Xi_{12} = -e^{4i\gamma_c\tau}(J_2 - J_1)(J_1 - J_3)\Omega_1^2 - 4e^{4i\gamma_c\tau}J_2 J_3\gamma_c^2$$

$$+ 2ie^{2i\gamma_c\tau}(J_2 + J_3)\gamma_c\kappa_c + \kappa_c^2,$$

$$\chi_{21} = \chi_{31} = -(\alpha + \bar{\alpha})(J_3 - J_2),$$

$$\chi_{22} = -\frac{\bar{\alpha}}{\alpha}\chi_{32} = \bar{\alpha}(J_3 - J_2),$$

$$\Xi_{22} = \Xi_{32} = 2iJ_1\gamma_c + e^{-2i\gamma_c\tau}\kappa_c,$$

$$\chi_{23} = (J_2 - J_1)\left[2\alpha\bar{\alpha}(J_1 - J_3)\Omega_1 - (\alpha + \bar{\alpha})\kappa_c\right],$$

$$\Xi_{23} = \Xi_{33} = (J_1 - J_2)(J_1 - J_3)\Omega_1^2 + \kappa_c^2,$$

$$
\begin{aligned}
\chi_{24} = &\, \bar{\alpha}e^{2i\gamma_c\tau}(J_2 - J_1) \\
&\times \left[\alpha e^{2i\gamma_c\tau}(J_1 - J_3)\Omega_1 - 2ie^{2i\gamma_c\tau}J_2\gamma_c - \kappa_c\right],
\end{aligned}
$$

$$
\begin{aligned}
\Xi_{24} = \Xi_{34} = &-e^{4i\gamma_c\tau}(J_2 - J_1)(J_1 - J_3)\Omega_1^2 \\
&- 4e^{4i\gamma_c\tau}J_2 J_3\gamma_c^2 \\
&+ 2ie^{2i\gamma_c\tau}(J_2 + J_3)\gamma_c\kappa_c + \kappa_c^2,
\end{aligned}
$$

$$\chi_{32} = -\alpha(J_3 - J_2),$$

$$\chi_{33} = \alpha(J_1 - J_3)\left[(\alpha + \bar{\alpha})(J_2 - J_1)\Omega_1 - 2\alpha\bar{\alpha}\kappa_c\right],$$

$$
\begin{aligned}
\chi_{34} = &\, \alpha\bar{\alpha}e^{2i\gamma_c\tau}(J_1 - J_3) \\
&\times \left[e^{2i\gamma_c\tau}(J_2 - J_1)\Omega_1 - 2i\alpha e^{2i\gamma_c\tau}J_3\gamma_c - \alpha\kappa_c\right].
\end{aligned}
\tag{41}
$$

Note, again, that γ_c can be obtained from Eq. (11) and the relation between κ_c and γ_c is given in Eq. (12). The Hopf bifurcation is supercritical if $\text{Re}(\Lambda_2) < 0$, and it is subcritical if $\text{Re}(\Lambda_2) > 0$.

5 Results and discussion

First, to obtain the stability conditions for the spin about the $\hat{b}_1$ axis which corresponds to the intermediate spin with the delayed feedback control in Eq. (2) for $\tau = 1$ s, we select J_2 and J_3 to be $J_2 = 10$ kg.m^2 and $J_3 = 30$ kg.m^2. Then, we either fix Ω and change J_1, or vice versa. This way, the stability chart can be expressed in a one-dimensional format where κ varies along the horizontal axis as in [22]. Note that $\alpha_0 < 0$ corresponds to the intermediate spin which is unstable without controller. The stability conditions given in Eqs. (19), (25), and (26) are visualized in Figs. 5–11 for $\tau = 1$ s and different values of $\mathbf{J}$ and Ω_1. The vertical blue and red lines in the figures correspond to $\kappa = \frac{\pi J_1}{2\tau}$ and $\kappa = \sqrt{-\alpha_0 J_2 J_3}$, respectively [Eqs. (19) and (25)], whereas the black curve
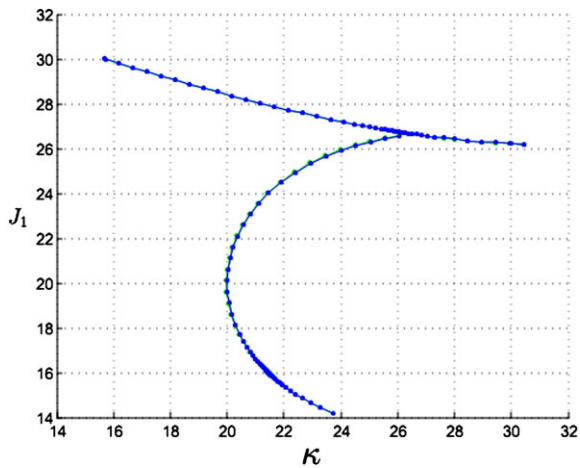
Fig. 16 Bifurcations in the $J_1 - \kappa_c$ parameter plane for the moments of inertia $J_2 = 10$ kg.m^2, $J_3 = 30$ kg.m^2, nominal spin rate $\Omega_1 = 2 \frac{\text{rad}}{\text{s}}$, and $\tau = 1$ s

represents f in Eq. (26). The shaded areas in the figures represent the stable regions where Eqs. (19), (25), and (26) are simultaneously satisfied. Permitted values of the control gain κ contain those which lie between the blue and red lines, and, at the same time, those for which the value of f calculated in Eq. (26) is non-positive. One can observe that for a fixed Ω_1, the stability area becomes narrower as J_1 increases to 20 kg.m^2, and that as J_1 becomes greater than 20 kg.m^2, two stable regions start to appear. In Fig. 8, for instance, it can be seen that for $\Omega_1 = 2 \frac{\text{rad}}{\text{s}}$ and $J_1 = 20$ kg.m^2, the system is stable only if $\kappa = 20$. It can also be seen that as the nominal spin rate Ω_1 increases from 0 to 2 $\frac{\text{rad}}{\text{s}}$ for the fixed value of $J_1 = 20$ kg.m^2, the range of the control gain κ that stabilizes the system becomes narrower.
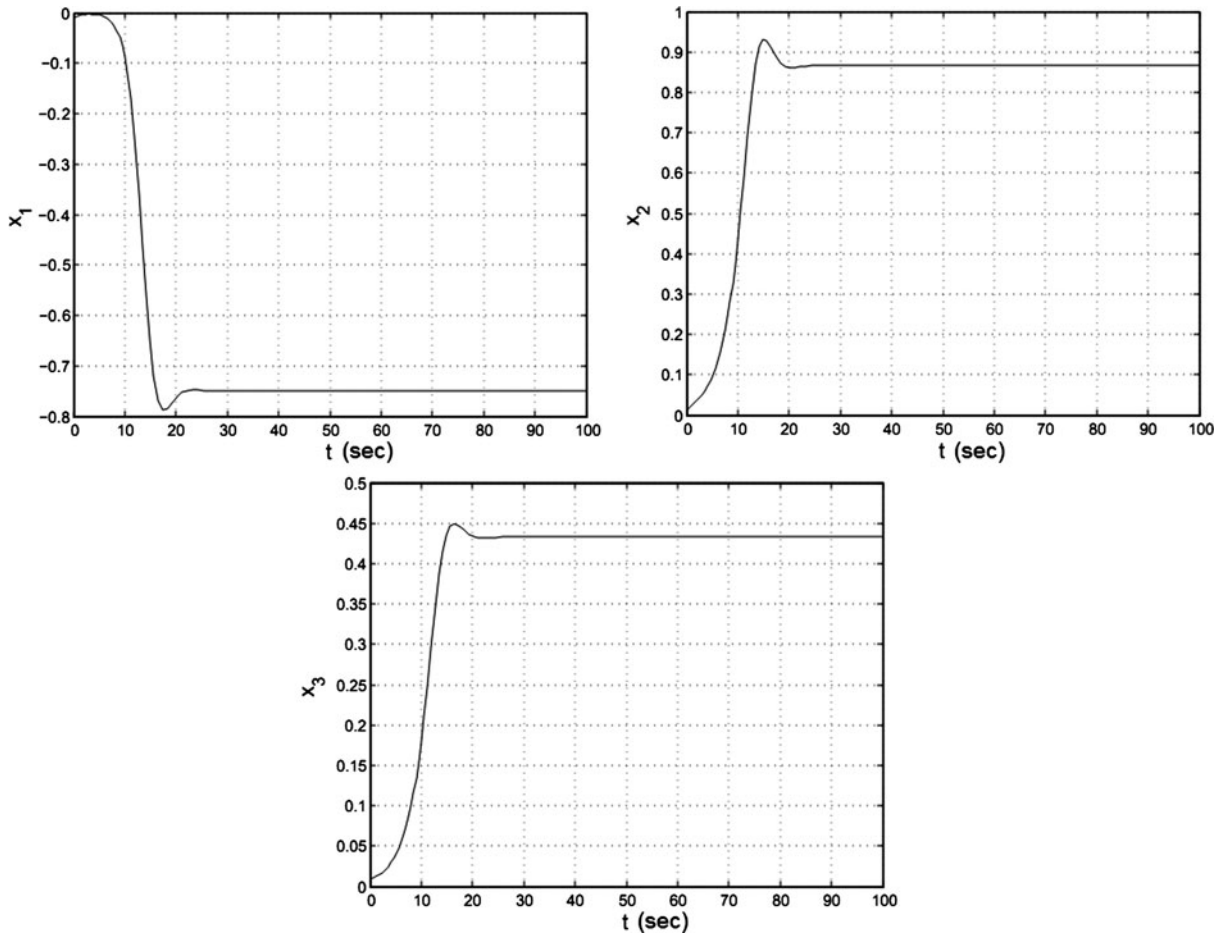
Fig. 17 Time series for the inertia matrix $\mathbf{J} = \text{diag}([14, 10, 30])$ kg.m^2, control gain $\kappa = 10$, nominal spin rate $\Omega_1 = 2 \frac{\text{rad}}{\text{s}}$, and $\tau = 0.01$ s
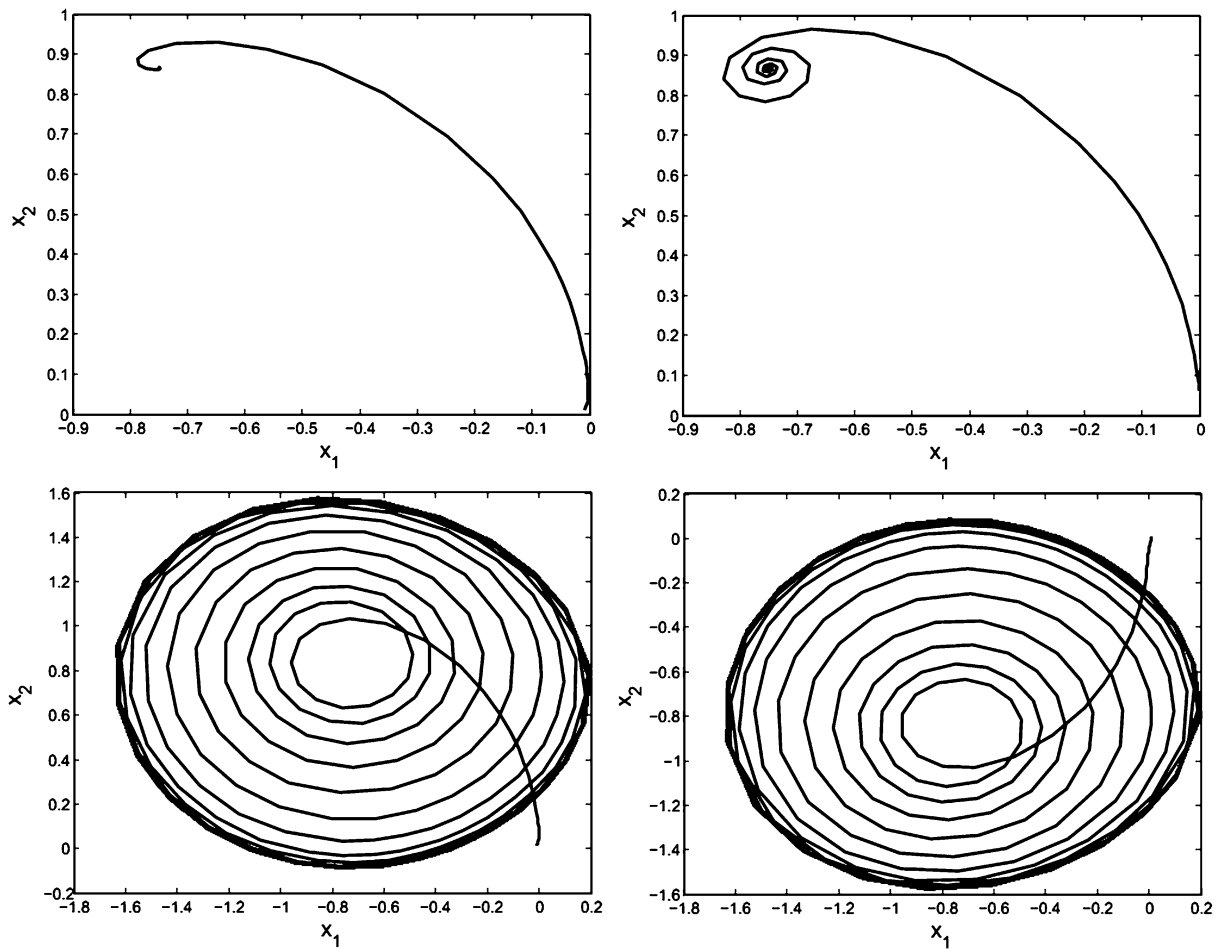
Fig. 18 The nontrivial equilibrium solution is stable node for the system with non-delayed feedback control (*top left*), stable spiral for $\tau = 0.8$ s (*top right*), and stable limit cycle for $\tau = 1$ s (*bottom left*). The second limit cycle (*bottom right*) can be achieved by starting from $\mathbf{x}_0 =$ $[0.01, 0.01, -0.01]^T$, while for the rest of the simulations, $\mathbf{x}_0 = [-0.01, 0.01, 0.01]^T$. The results are shown for the inertia matrix $\mathbf{J} = \text{diag}([14, 10, 30])$ kg.m^2, control gain $\kappa = 10$, and nominal spin rate $\Omega_1 = 2 \frac{\text{rad}}{\text{s}}$

Next, we utilize DDE-BIFTOOL [23, 24] to obtain the (infinite number of) eigenvalues of the delayed system (4) as the control parameter κ changes. The real part of the eigenvalue λ of the system (4) is plotted versus the control parameter κ in Figs. 12 and 13 for $\tau = 0.01$ s, and in Figs. 14 and 15 for $\tau = 1$ s. Note that by assuming $\tau = 0.01$ s in the simulations, the system is considered to be almost non-delayed.

One can observe that the stability of the trivial solution based on the negativeness of the real part of the eigenvalues for the almost non-delayed case ($\tau = 0.01$ s) in Figs. 12 and 13 agrees with the bifurcation diagrams given in Figs. 1 and 2 obtained for the corresponding non-delayed system where the

trivial solution becomes stable and remains so after κ reaches a specific value. Whereas, when the time delay is added, the trivial solution becomes stable for the respective value of κ, but loses stability after κ continues to grow. When $\kappa < 0$, the system exhibits unbounded motion as is expected from the bifurcation charts shown in Figs. 1–3 because there is no equilibrium solution other than the trivial solution which is a repellor. The stability regions defined by the negativeness of the real part of the eigenvalues of the delayed system with $\tau = 1$ s shown in Figs. 14 and 15 agree, respectively, with those obtained in Figs. 6 and 8 using the strategy given in Sect. 3.3. Figure 16 shows the bifurcation diagram in the $J_1 - \kappa_c$ parameter plane
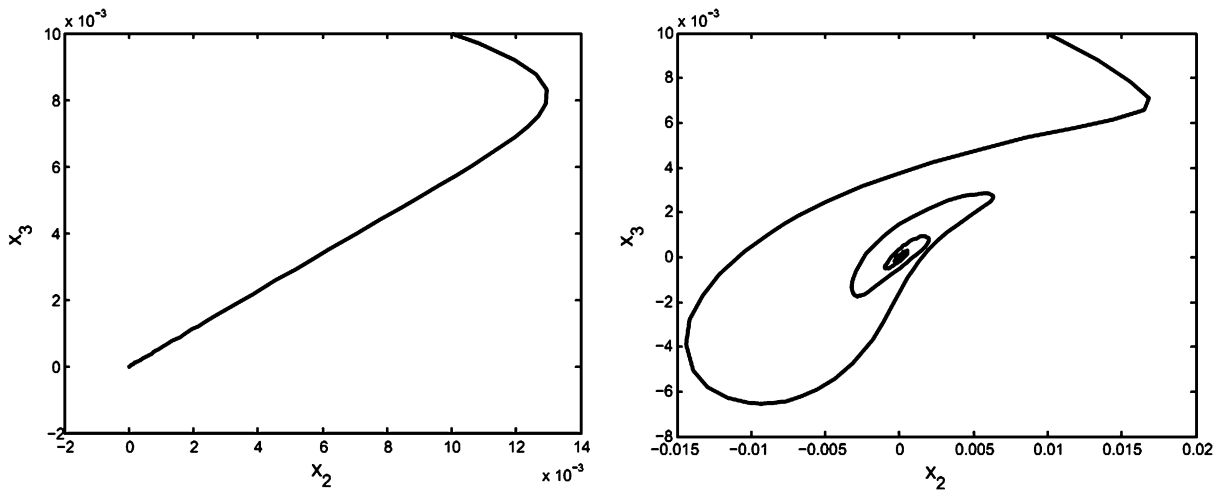
Fig. 19 The trivial solution is a stable node for the non-delayed system (*left*), and a stable spiral for $\tau = 1$ s (*right*). The results are shown for the inertia matrix $\mathbf{J} = \text{diag}([14, 10, 30])$ kg.m^2, control gain $\kappa = 20$, and nominal spin rate $\Omega_1 = 2 \frac{\text{rad}}{\text{s}}$
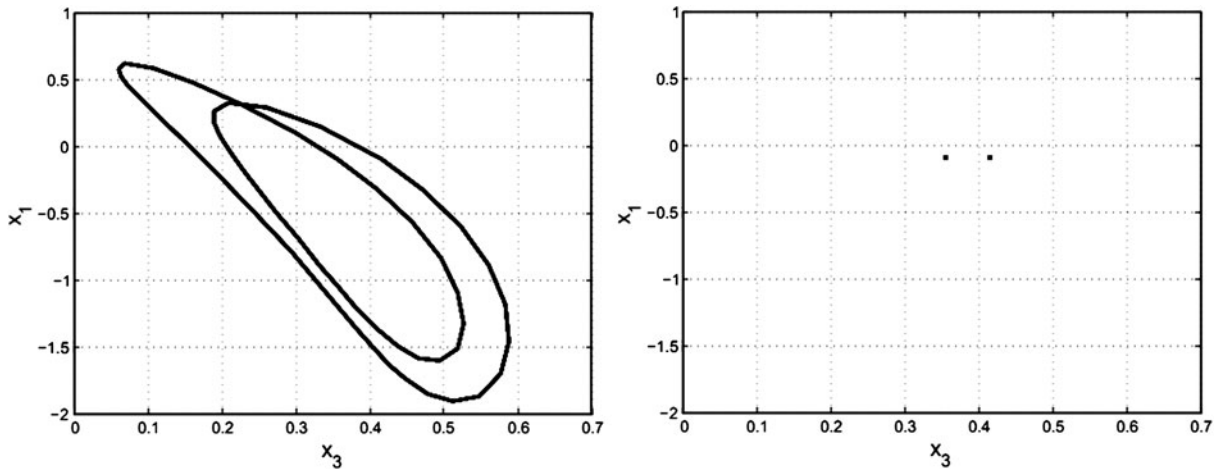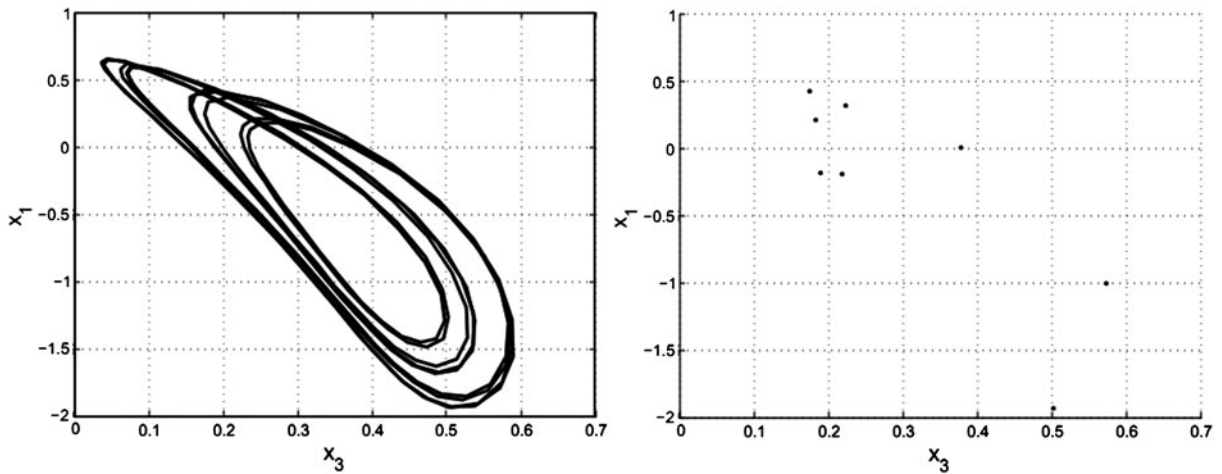

Fig. 20 Period-2 motion at $\tau = 1.1$ s for the inertia matrix $\mathbf{J} = \text{diag}([14, 10, 30])$ kg.m^2, control gain $\kappa = 10$, and nominal spin rate $\Omega_1 = 2 \frac{\text{rad}}{\text{s}}$

where it can be seen that a bifurcation of co-dimension 2 happens at $(\kappa_c, J_1) = (20, 20)$. Note that the stable node(s) obtained by the bifurcation charts shown in Fig. 1 at $\kappa = 10$ agree with the simulated results shown in Fig. 17. Note that the initial conditions are assumed to be $\mathbf{x}_0 = [-0.01, 0.01, 0.01]^T$ for the simulated results shown, unless mentioned otherwise.

Furthermore, the simulated results in Fig. 18 produced for $\mathbf{J} = [14, 10, 30]$ kg.m^2, $\Omega_1 = 2 \frac{\text{rad}}{\text{s}}$, and different time delays of $\tau = 0$, $\tau = 0.8$ s, and $\tau = 1$ s indicate that the other equilibrium solution which is stable node for the system with non-delayed feedback con-

trol becomes stable spiral as the time delay increases from 0 to 0.8 s, and it becomes stable limit cycle as the time delay increases from 0.8 s to 1 s. This can be verified by the fact that for $\mathbf{J} = [14, 10, 30]$ kg.m^2 and $\Omega_1 = 2 \frac{\text{rad}}{\text{s}}$, Eq. (11) has a root for γ_c only if $\tau \geq 0.925$ s. On the other hand, according to Figs. 1 and 19, the trivial solution is stable node for $J_1 = 14$ kg.m^2 and $\kappa = 20$ for the non-delayed system, while it becomes a stable spiral for the same value of κ and $\tau = 1$ s. Therefore, the bifurcation type changes from supercritical pitchfork bifurcation to supercritical Hopf as the time delay is added to the system. Note

Fig. 21 Period-8 motion at $\tau = 1.1095$ s for the inertia matrix $\mathbf{J} = \mathrm{diag}([14, 10, 30])$ kg.m^2, control gain $\kappa = 10$, and nominal spin rate $\Omega_1 = 2 \frac{\mathrm{rad}}{\mathrm{s}}$
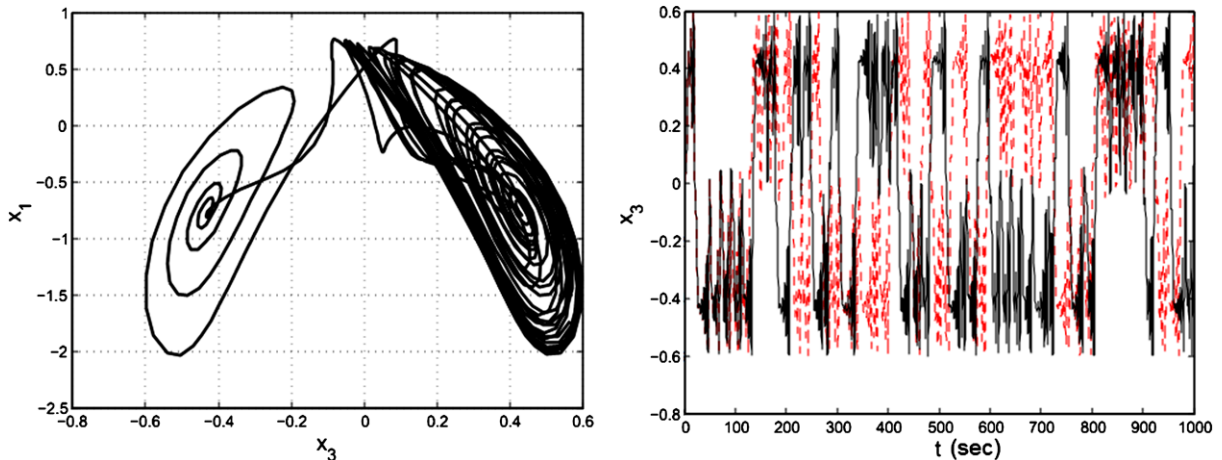
Fig. 22 The strange attractor of the chaotic response at $\tau = 1.15$ s is shown in *left*. The sensitivity to initial conditions is shown in *right* where the initial conditions are $\mathbf{x}_0 = [0.01, 0.01, 0.01]^T$ (*solid*) and $\mathbf{x}_0 = [0.0101, 0.0101, 0.0101]^T$

(*dashed*). The results are shown for the inertia matrix $\mathbf{J} = \mathrm{diag}([14, 10, 30])$ kg.m^2, control gain $\kappa = 10$, and nominal spin rate $\Omega_1 = 2 \frac{\mathrm{rad}}{\mathrm{s}}$

that according to Fig. 1, for $\kappa = 10$ there are two equilibrium solutions to which the trajectories may travel depending on the chosen initial conditions. For instance, when $\tau = 1$ s there are two stable limit cycles which are shown in Fig. 18.

As can be understood, the system is periodic for $\tau = 1$ s. Let κ be fixed at $\kappa = 10$. According to the simulations, when the time delay becomes slightly greater than $\tau = 1$ s the system exhibits period-doubling bifurcation, and becomes chaotic via this phenomenon. The sequential period-doubling occurs

at $\tau = 1.1$ s (period-2), $\tau = 1.105$ s (period-4), $\tau = 1.1095$ s (period 8), and $\tau = 1.1104$ s (period 16). One can see that the sequential bifurcation points given above are consistent with the Feigenbaum universal constant. The 2- and 8-periodic responses are shown in Figs. 20 and 21, respectively. The chaotic attractor for $\tau = 1.15$ s is shown Fig. 22, where the chaotic motion is verified via the sensitivity of the response to the initial conditions. Note that the trajectories in Fig. 22-left are shown for the last 10 % of the elapsed time.

6 Conclusion

In this study, a linear delayed feedback control law was introduced to stabilize the relative angular motion of spacecraft about an equilibrium state, which can be the spin about any of the principal axes of the spacecraft, regardless of the external torques. Since the spin about the centroidal principal axis of intermediate moment of inertia is generally unstable if no controller is used, the specific concentration was on the intermediate spin. The stability conditions obtained via delay dependent and delay independent stability analysis were verified by means of continuation software. AUTO continuation software was applied to the non-delayed closed-loop system to produce branches of equilibria for varying control gain, while DDE-BIFTOOL continuation software was used to obtain the (infinite number of) eigenvalues of the delayed closed-loop system. Furthermore, the method of multiple time scales was employed to provide the normal form of the Hopf bifurcation. The stability and bifurcation of the system was studied and compared with the simulation results. The results indicate that while a sufficiently large control gain can satisfy (global asymptotic) stability of the non-delayed closed-loop system, stability of the delayed closed-loop system requires accurate selection of the control gain. As the critical case, if the intermediate moment of inertia equals the average of the two other moments of inertia, then there is only one value for the control gain for which the intermediate spin stability can be attained for the system with a non-negligible delay. Finally, the period-doubling route to chaos was observed via increasing the time delay from a certain amount. As a future work, bifurcation analysis of delayed spin stabilization of a dual-spin spacecraft can be considered where two subsystems have relative spin motion with respect to each other.

Appendix

Critical frequency of the characteristic equation in Sect. 3.1

Substituting for k_p from Eq. (8) into Eq. (10a) on the stability boundary, the term $\kappa_c^2 \cos 2\gamma_c\tau$ appears

which, using trigonometric identities, can be expressed as

$$\kappa_c^2 \cos 2\gamma_c\tau = \kappa_c^2\big(1 - 2\sin^2\gamma_c\tau\big)$$
$$= \kappa_c^2 - 2(\kappa_c\sin\gamma_c\tau)^2. \quad (A.1)$$

Solving Eq. (10b) for κ_c gives

$$\kappa_c = \frac{J_2 + J_3}{2}\frac{\gamma_c}{\sin\gamma_c\tau}. \quad (A.2)$$

Substituting Eq. (A.2) into Eq. (A.1), one can obtain

$$\kappa_c^2 \cos 2\gamma_c\tau = \frac{(J_2+J_3)^2}{4}\frac{\gamma_c^2}{\sin^2\gamma_c\tau} - 2\frac{(J_2+J_3)^2}{4}\gamma_c^2$$
$$= \frac{(J_2+J_3)^2}{4}\gamma_c^2\left(\frac{1}{\sin^2\gamma_c\tau} - 2\right). \quad (A.3)$$

Substituting Eqs. (A.2) and (A.3) into Eq. (10a), it becomes

$$-\gamma_c^2 + \gamma_c^2\left(\frac{J_2+J_3}{J_2 J_3}\right)\frac{J_2+J_3}{2}$$
$$+ \frac{(J_2+J_3)^2}{4J_2 J_3}\gamma_c^2\left(\frac{1}{\sin^2\gamma_c\tau} - 2\right)$$
$$= \frac{(J_3-J_1)}{(J_1-J_2)}J_2 J_3 \Omega_1^2, \quad (A.4)$$

where Eq. (8) is used to substitute for α, k_p, and k_d in terms of κ and the parameters of the system. Therefore, the critical frequency corresponding to κ_c can be obtained via

$$\gamma_c = \Omega_1\sqrt{\frac{(J_3-J_1)(J_1-J_2)}{-1+\frac{1}{2}(J_2+J_3)^2[1+\frac{1}{2}(\frac{1}{\sin^2\gamma_c\tau}-2)]}}$$
$$= \Omega_1\sqrt{\frac{(J_1-J_3)(J_1-J_2)}{1-\frac{(J_2+J_3)^2}{4\sin^2\gamma_c\tau}}}, \quad (A.5)$$

or, after using Eq. (A.2), the critical frequency can be expressed in terms of κ_c as

$$\gamma_c^2 = \frac{1}{J_2 J_3}\big[\kappa_c^2 + \Omega_1^2(J_3-J_1)(J_2-J_1)\big]. \quad (A.6)$$

References

1. Albu, I., Neamtu, M., Opris, D.: Dissipative mechanical systems with delay. Tensor **67**, 1–27 (2006)

2. Albu, I., Neamtu, M., Opris, D.: The dynamical rigid body with memory. In: Balkan Society of Geometers (BSG) Proceedings of International Conference of Differential Geometry Dynamical Systems (DGDS), October 5–7, 2007, vol. 15, pp. 1–10. Geometry Balkan Press, Bucharest (2008)

3. Ramnath, R.V.: Multiple Scales Theory and Aerospace Applications. AIAA, Reston (2010)

4. Tao, Y.C., Ramnath, R.V.: Satellite Attitude Prediction by Multiple Time Scales Method. The Charles Stark Draper Laboratory, Cambridge (1975)

5. Alfriend, K.T.: Magnetic attitude control system for dual-spin satellites. AIAA J. **13**(6), 817–822 (1975)

6. Gebman, J.R., Mingori, D.L.: Perturbation solution for the flat spin recovery of a dual-spin spacecraft. AIAA J. **14**(7), 859–867 (1976)

7. Chunodkar, A., Akella, M.: Attitude stabilization with unknown bounded delay in feedback control implementation. J. Guid. Control Dyn. **34**(2), 533–542 (2011)

8. Samiei, E., Nazari, M., Butcher, E., Schaub, H.: Delayed feedback control of rigid body attitude using neural networks and Lyapunov–Krasovskii functionals. In: AAS/AIAA Spaceflight Mechanics Meeting, Charleston, SC (2012). Paper No. 12-168

9. Nazari, M., Butcher, E., Schaub, H.: Spacecraft Attitude Stabilization using Nonlinear Delayed Multi-Actuator Control and Inverse Dynamics. J. Guid. Control Dyn. (2013). doi:10.2514/1.58249

10. Nayfeh, A.: Method of Normal Forms. Wiley, New York (1993)

11. Bambusi, D.: Galerkin averaging method and Poincaré normal form for some quasilinear PDEs. Ann. Sc. Norm. Super. Pisa, Cl. Sci. **4**(5), 669–702 (2005)

12. Butcher, E.: Normal forms for high co-dimension bifurcations of nonlinear time-periodic systems with nonsemisimple eigenvalues. Nonlinear Dyn. **30**, 29–53 (2002)

13. Nayfeh, A.: Order reduction of retarded nonlinear systems—the method of multiple scales versus center-manifold reduction. Nonlinear Dyn. **51**, 483–500 (2008)

14. Xu, J., Lu, Q.: Hopf bifurcation in a time-delayed lienard equation. Int. J. Bifurc. Chaos Appl. Sci. Eng. **9**(5), 939–951 (1999)

15. Faria, T.: Normal forms and Hopf bifurcation for partial differential equations with delays. Trans. Am. Math. Soc. **352**(5), 2217–2238 (2000)

16. Das, S., Chatterjee, A.: Multiple scales without center manifold reductions for delay differential equations near Hopf bifurcations. Nonlinear Dyn. **30**, 323–335 (2002)

17. Kielhöfer, H.: Bifurcation Theory: an Introduction with Applications to Partial Differential Equations. Springer, New York (2004)

18. Doedel, E., Champneys, A.T.F., Kuznetsov, Y., Oldeman, B., Paffenroth, R., Sandstede, B., Wang, X., Zhang, C.: AUTO-07p: Continuation and Bifurcation Software for Ordinary Differential Equations. Concordia University Montreal, Canada (2007)

19. Insperger, T., Stépán, G.: Semi-Discretization for Time-Delay Systems: Stability and Engineering Applications. Springer, New York (2011)

20. Bers, L., John, F., Schechter, M.: Partial differential equations. In: Lectures in Applied Mathematics, vol. 3A, pp. 1–343. Wiley, New York (1964)

21. Nayfeh, A.: Problems in Perturbation. Wiley, New York (1985)

22. Schaub, H., Junkins, J.: Analytical Mechanics of Space Systems. AIAA, Reston (2009)

23. Engelborghs, K., Luzyanina, T., Samaey, G.: DDE-BIFTOOL v. 2.00: A Matlab Package for Bifurcation Analysis of Delay Differential Equations. Department of Computer Science. K.U. Leuven, Technical Report TW-330, Leuven, Belgium (2001)

24. Engelborghs, K., Luzyanina, T., Roose, D.: Numerical bifurcation analysis of delay differential equations using DDE-BIFTOOL. ACM Trans. Math. Softw. **28**(1), 1–21 (2002)